Electrical Power and Energy Systems 160 (2024) 110123

Contents lists available at ScienceDirect

International Journal of Electrical Power and Energy Systems

journal homepage: www.elsevier.com/locate/ijepes

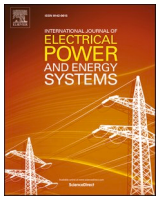

Reduction of power transmission losses in high-speed rail systems through efficient scheduling

Jesus Riego-Martinez [a], Marcelo Perez-Alonso [a], Oscar Duque-Perez [b,*]

[a] Renfe, Madrid 28045 Spain
[b] Electrical Engineering Department, University of Valladolid, 47011 Spain

ARTICLE INFO

Keywords:
Railway engineering
Rail transportation
Energy consumption

ABSTRACT

The need to reduce overall energy consumption motivates the search for ways to improve energy use by transportation. Electrification has helped to significantly reduce the energy intensity of rail transportation. On today's high-speed lines, power flows between trains and traction transformers are generally transmitted through the 2x25 electrification system. Although most of the energy provided to the railway system is consumed by the moving trains, a part of the energy is lost in the electrification system itself. In this study, dynamic computer simulations of realistic high-speed rail operating scenarios are developed and the energy losses in the electrification system are evaluated. The results show that power transmission losses are significant, and their value depends on the operation scenario. Finally, a method for selecting the minimum transmission loss operating scenarios is proposed, without modifying the transportation capacity offered or altering the resources required for the operation of a high-speed rail.

1. Introduction

Although rail is considered to be one of the most energy-efficient modes of transportation, its high share of overall transportation activity makes the search for techniques to reduce its energy consumption and associated gas emissions a key objective of current research work. The expansion of the electrification of railway lines over the last decades has significantly improved the energy intensity of rail transportation. According to data from the International Energy Agency, the specific consumption of rail passenger transportation has been reduced from 375 kJ/pkm in 1975 to 200 kJ/pkm in 2015 [1].

In high-speed rail systems, several strategies are being implemented to reduce energy consumption. These measures can be grouped according to the focus of their efforts: infrastructure, rolling stock and operation. Measures focusing on infrastructure and rolling stock involve long implementation times and high investment costs, being often deferred to the medium to long term, as the opportunity to undertake them must be carefully sought [2]. In contrast, most energy efficiency improvement measures based on changes in operation can be implemented within a short timeframe and with low associated costs [3].

Numerous references on operational strategies to reduce energy consumption can be found in the literature (see [4,5] for reviews on this subject). Energy efficient train control (also known as eco-driving) is reported as an effective way to reduce energy consumption; in [6] a thorough review on eco-driving is presented encompassing different railway systems, while [7] is limited to high-speed systems. Acting on the timetable has also been addressed in previous works: A first approach is based on adjusting the timetable to make the best possible use of efficient driving [6]. A second approach is to act on the timetable with proposals such as [8] where the aim is to recalculate timetables in the face of disturbances in order to minimise delays and consumption, [9] where the robustness of the schedule is analysed, or [10] where the adjustment of the schedule tries to reduce peaks in substations. Because of its energy-savings potential, it has been widely considered the option of maximising regenerative energy, using the braking energy to power other trains on the line [11]. This energy efficiency improvement has been especially studied in urban transport where high traffic density stimulates the search for energy saving opportunities. Numerical methods have been applied [12–17], with an emphasis on heuristic [18–25] and artificial intelligent techniques [21,26]. Some of these studies also consider efficient driving, [12,13,15,25,27] incorporate the possibility of delays in the study, [22] considers interconnected lines while [23] considers the possibility of power interruptions, [16] includes the possibility of energy storage in the optimisation. Lately, the

* Corresponding author.
E-mail address: oscar.duque@uva.es (O. Duque-Perez).

https://doi.org/10.1016/j.ijepes.2024.110123
Received 8 March 2024; Received in revised form 25 June 2024; Accepted 3 July 2024
Available online 13 July 2024

analysis of these high traffic density services has incorporated the need to consider them as cyclic services [28], taking as an objective to minimise the cyclic time that takes into account the times of the outward and return journeys as well as the waiting times at the origin and end stations [29]. Subsequently, the scope of the research work has been extended to include all elements of the railway electrical system. This overview presents two improvements over previous work: it allows the evaluation of power flows applying electric braking to a nearby train in traction [17,24] and accounts for transmission losses in the electrification system [14].

As reflected in the previous paragraphs, the adjustment of timetables to optimise the operation of the railway system has been extensively dealt with in urban systems, where the traffic density is very high. However, it has been much less treated in interurban systems, where the density is much lower, although it must be taken into account that in these cases the electrical losses are significantly higher. Although there are few references in the literature that account for losses in the electrification system, power transmission losses are inherent to electrified railway transportation and should not be ignored [30]. Some proposals can be found regarding DC trains: [31] presents a procedure to obtain robust timetables by minimising the energy consumption of trains due to delays; [32] computes the electrical losses by means of pre-set coefficients assigned to various parts of the system such as the line and the substation; in [33], a schedule adjustment proposal is presented to make the best use of regenerative energy and, in addition, to shave peak power, but not take into account the losses in the electrical system; in [34] a procedure is presented for optimizing energy exchanges between trains by accelerating and braking to take advantage of possible delays in trains included in the preset schedule; in [35] the rescheduling has as objective to avoid overloads in the supply system. However, less similar research on high-speed lines has been published. In the case of urban railways –typically fed in direct current– the energy regenerated in braking is dissipated if the space–time coincidence of the trajectories of two trains does not occur. On the contrary, the electrical substations that feed the high-speed lines –in single-phase alternating current– are reversible and admit return power flows from the braking trains to the high-voltage supply network. Furthermore, published papers on energy-efficient scheduling on high-speed lines rarely consider power transmission losses in the electrification system; [36] presents a multi-objective problem (to minimize the average travel time of trains, the energy consumption and the delayed times) solved using an heuristic optimization algorithm but only the traction energy consumption is considered; in [37] it is proposed to modify the trajectory as well as the timetable, but this implies changes difficult to implement, especially in competitive markets. Typically, a high-speed train running within an electrification section is powered from a traction substation by single-phase alternating current. For most of the time, the substation exchanges power individually with a single train –transferring power from the high-voltage supply network in the traction phases and returning power when the train applies regenerative braking. These power exchanges are subject to transmission losses. In fact, power transmission losses can reach values close to 5 % of the energy supplied to the high-speed railway system as estimated in [38]. Eventually, another train may run simultaneously within the same electrification section. As explained in this paper, this concurrence modifies in several ways the power exchanges and the consequent transmission losses that occur in the electrification system.

To fill this gap, this paper evaluates the performance of the electrification system of a high-speed line operated in different scenarios of a transportation plan based on periodic timetables. Power transmission losses are calculated by simulating the operation of the complete railway system. By comparing the results of different scenarios –without varying train speed profiles–, the effect of scheduling adjustment on energy loss is assessed. The results show that it is possible to reduce transmission losses in the electrification system by up to 31.55 % by modifying the departure times of some services.

The paper is organized as follows. Section II presents the mathematical basis of the models used to describe rail traffic, the mechanics of train movement, the electromechanical conversion in the train traction chain and the electrification system. Section III details the algorithms used for the numerical resolution of the models. The case studies in Section IV show the importance of loss control through service scheduling. Finally, Section V draws the main conclusions.

2. Mathematical basis

The operating scenarios to be studied consist of a set of trains running simultaneously along a high-speed railway line. A first mathematical model represents rail traffic by defining the departure times and trajectories of all the services that make up the transportation plan. The dynamics of the movement of each train and the electromechanical conversion in its traction chain are represented by a second model. Finally, a third model reproduces the operation of the railway electrification system that feeds the line on which all the trains run.

2.1. Rail traffic

The scheduling of a transportation plan between two ends of a railway line is based on two type trajectories, one for each direction. By convention, consecutive odd numbers are used to designate the services running in one direction and consecutive even numbers to designate the services in the opposite direction. In this way, all the odd services are programmed to circulate following the type 1 trajectory $x_{type,1}$, and all the even services following the type 2 trajectory $x_{type,2}$. Both types of trajectories must be carefully designed to be feasible and reproducible by the trains under various operating conditions [39].

In a transportation plan based on periodic schedules, the departure and arrival times represent periodic events. As shown in (1) and (2), any pair of consecutive odd –or even– services are separated by a headway T_H. In addition, the departure times of the even services are temporarily offset from the departure times of the odd services by a layover time T_L. Consequently, passengers are served by transportation services that follow a regular and simple pattern. According to the Marry-Go-Round paradigm, the fleet size is quasi-inverse proportional to the value of the headway. Therefore, a trade-off between the expected demand and the existing constraints for the operation must be made to set the value of headway T_H [28].

$$x_{2m+1}(t) = x_{type,1}(t - mT_H) \tag{1}$$

$$x_{2m+2}(t) = x_{type,2}(t - T_L - mT_H) \tag{2}$$

On the other hand, different values for T_L in (2) temporarily shift the scheduled departure times of the even services. Given the periodic structure of the transportation plan, the variation of T_L within the interval [0, T_H) results in a complete set of different operating scenarios. If the operation is carried out on a double track line, the variation of T_L does not compromise the capacity of the infrastructure, nor does it require a change in the size of the available fleet. Therefore, for each value of the headway T_H, it is possible to generate a complete set of equivalent operating scenarios. These equivalent scenarios offer the same transportation capacity and, in general, respect the same operating constraints [40].

2.2. Train motion

The trajectory x_n described by the train providing service n is the result of the forces acting as it travels along the track. In the models commonly used in literature, the train is considered a point mass moving along a one-dimensional space, i.e., the track. Recently, more accurate simulation models have been developed that overcome this simplification [41,42]. However, the study proposed in this paper requires the recurrent simulation of different operating scenarios to be compared.

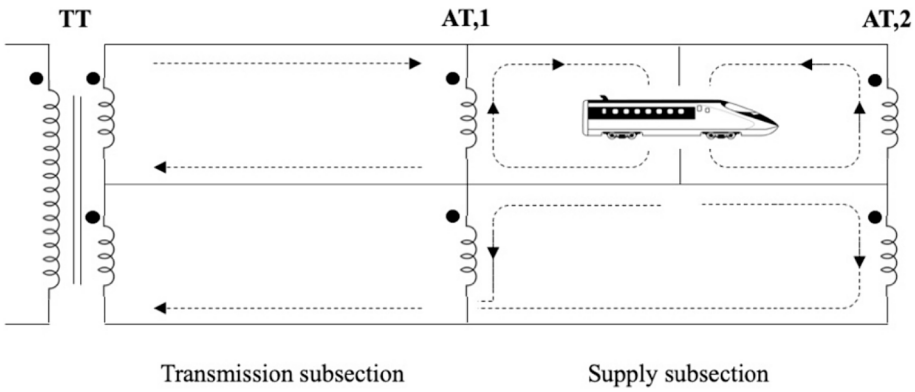

Fig. 1. Model of the 2x25 kV electrification system.

The search for a trade-off between simulation processing time and accuracy has led us to adopt the simplified model. Thus, the study of train dynamics can be reduced to the evaluation of two forces acting in the direction of train motion: the traction and braking force F_n and the forward resistance R_n.

The traction and braking force F_n is the result of the control performed on the traction chain of the train so that its actual trajectory conforms to the trajectory programmed for the service it provides. F_n control can be exercised manually by the driving staff or automatically by the train operation system. The driving resistance R_n is a negative force opposing the movement of the train. The total driving resistance R_n experienced by the train during its movement is the sum of the train's basic resistance $R_{n,basic}$ and the resistance due to infrastructure $R_{n,infra}$.

$$R_{n,basic}(t) = A + B\frac{dx_n}{dt} + C\left(\frac{dx_n}{dt}\right)^2 \tag{3}$$

$$R_{n,infra}(t) = m_{train}gi(t) + C_t\left(\frac{dx_n}{dt}\right)^2 \tag{4}$$

$R_{n,basic}$ is the resistance to forward motion experienced by the train when running on a horizontal, straight, open-air section, due to mechanical friction, aerodynamic friction, and air intake. $R_{n,basic}$ is usually expressed by the Davis formula (3) where A, B and C are specific to each type of train [41]. The resistance due to infrastructure $R_{n,infra}$ is the additional resistance that the train suffers when running on gradients and tunnels. The decline i can increase or reduce the value of infrastructure resistance. The value of the tunnel factor C_t in (4) depends on the geometrical characteristics of both the tunnel and the train [43].

As shown in (5), applying Newton's second law on the mass of the train m_{train} –including the inertial effect of the rotating masses in ξ– the Lomonossoff equation is obtained [44].

$$F_n(t) = \xi m\frac{d^2x_n}{dt^2} + R_n(t) \tag{5}$$

For the train to be accelerated, the active electrical power P_n captured through the pantograph must be converted into mechanical power by the traction chain. As can be seen in (7), the losses of this electromechanical conversion must be considered through the efficiency η.

$$P_n(t) = \frac{1}{\eta}F_n(t)\frac{dx_n}{dt} \tag{7}$$

Dynamic braking of high-speed trains combines the use of both air and electric brakes. Depending on the braking demand and the train speed at each instant, the brake control system determines the distribution of the braking force between the air and electric brakes [45]. During electric braking, the traction chain of the train reverses its operation and generates electric power. When the technical conditions set out in [46] are fulfilled, the regenerated electrical power can be fed back through the pantograph. As stated in (8), the active electrical power P_n during braking depends on the regeneration rate ρ_n and the efficiency η of the electromechanical conversion. The value of ρ_n establishes the portion of the braking power that is regenerated and fed back into the electrification system. The value of ρ_n is variable, as it depends on the brake blending and the receptivity of the electrification system. In both traction and electric braking, the value of η for trains with induction motors can be considered constantly ~ 0.86 [47].

$$P_n(t) = \frac{\rho_n(t)}{\eta}F_n(t)\frac{dx_n}{dt} \tag{8}$$

As can be seen in (9), the complex electrical power in the train's traction chain S_n consists of an active component and a reactive component. The power factor of the train λ_n determines the magnitude of its reactive power at each instant. For today's high-speed trains, the value of λ_n is close to unity over almost the entire active power range of the train. Lower values of λ_n only appear when P_n is reduced below 12.5 % of its nominal power [48].

$$S_n(t) = P_n(t)\left[1 + j\sqrt{1-\lambda_n^2(t)}\right] \tag{9}$$

2.3. Electrification system

The traction chains of today's high-speed trains are designed to accept single-phase alternating current captured through their pantograph and provided through a sequence of traction transformers [49]. Each traction transformer is connected to a single electrification section, which is isolated from adjacent sections by neutral zones. In general, it is assumed that the high-voltage supply network is sufficiently robust to consider the operation of each electrification section independently [50].

The secondary of traction transformers in the 2x25 kV electrification system –the most widespread system on today's high-speed railways– consists of two identical windings in series. The nominal voltages of the connection terminals are +25 kV on the overhead contact line, 0 kV on the rail and -25 kV on the negative feeder. Several traction autotransformers are located at regular intervals along each electrification section. Each autotransformer consists of two identical windings in series. The end terminals of each autotransformer are connected to the overhead contact line and the negative feeder, and the center tap to the rails. Each autotransformer draws most of the return current from its center tap to its end terminals. In this way, the return current extracted from the rails is diverted equally to the contact line and the negative feeder. This design drastically reduces the current flowing through the electrification system as the voltage difference between the contact line and the negative feeder is ~50 kV [51].

The operation of the 2x25 kV system can be approximated by a model widely used in the literature. As shown in Fig. 1, the model is

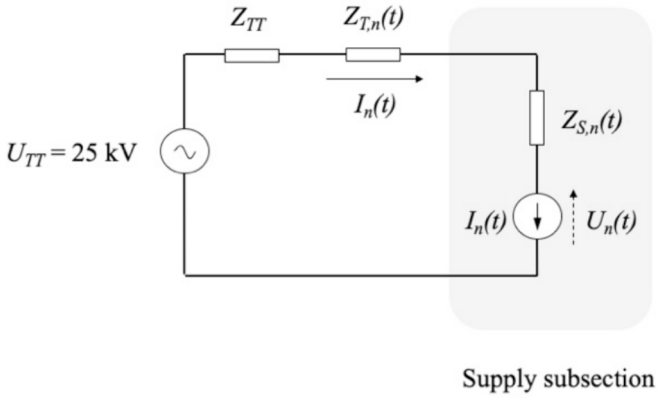

Fig. 2. Equivalent circuit for one section with one train in the approximate 2x25 kV system model.

based on two simplifications. First, each electrification section is represented by a concentrated parameter circuit obtained by the association of all equipotential conductors. Secondly, the model assumes that most of the current is drained by the two autotransformers closest to the train position. The residual current not drained by the autotransformers is conducted along the rails to the traction transformer. The accuracy achieved with these simplifications is acceptable for the evaluation of energy losses in the electrification system [52]. Therefore, this method is a suitable tool for the comparison of energy losses between different operating scenarios.

In addition, the operation of the electrification elements is modelled as follows:

Traction transformer. The high voltage supply network and the traction autotransformer are represented by means of a Thevenin equivalent circuit. As stated above, it is assumed that the supply network is sufficiently robust. Then, the equivalent circuit can be reduced to two ideal 25 kV voltage sources and the short-circuit impedance of the transformer Z_{TT}. The impedance of the traction transformer will contribute to the impedance of the transmission subsection, as shown in the following paragraphs.

Autotransformers. Since the two windings of the autotransformer are designed for the same voltage, i.e. 25 kV, they have the same number of turns and the transformation ratio is 2:1. Ideally, it is assumed that there is no loss of magnetic flux between the two windings of each autotransformer. Consequently, according to Kirchhoff's current law, the return current reaching at the central tap of each autotransformer is split into two equal parts, as seen in Fig. 1. Depending on the position of the train, the impedance of each autotransformer will contribute to the impedance of each subsection (transmission or supply) as specified in the following paragraphs.

Traction chain. The train is represented by a time-varying current source. The instantaneous value of I_n is related in (10) to the electrical power of the train S_n.

$$S_n(t) = U_n(t)I_n^*(t) \tag{10}$$

Taking advantage of the symmetries derived from the model of the two series windings of the secondary of the traction transformer and the autotransformers, the meshes of the circuit shown in Fig. 1 can be simplified into the equivalent circuit illustrated in Fig. 2 [53].

As can be seen in the model depicted in Fig. 2, I_n flows between the traction transformer and the train through the impedance of the transmission subsection $Z_{T,n}$ and the impedance of the supply subsection $Z_{S,n}$. Since the voltage at the traction transformer U_{TT} is assumed constant and equal to 25 kV, the voltage U_n and the current I_n of the train are related in (11) and (12) through the impedance of its traction circuit Z_n.

$$25 = U_n(t) + [Z_{TT} + Z_n(t)]I_n(t) \tag{11}$$

$$Z_n(t) = Z_{T,n}(t) + Z_{S,n}(t) \tag{12}$$

In the approximate electrical model used in this work, the values of $Z_{T,n}$ and $Z_{S,n}$ are derived from the positions of the transformer and autotranformers, x_{TT}, $x_{AT,1}$ and $x_{AT,2}$, in (13) and (14). The parameters Z_α, Z_β and Z_γ are characteristic values related to the impedances of the equivalent conductors resulting from each particular electrification system, as defined in [54].

$$Z_{T,n}(t) = Z_\alpha(x_{AT,1} - x_{TT}) \tag{13}$$

$$Z_{S,n}(t) = Z_\beta\left[x_n(t) - x_{AT,1}\right] - Z_\gamma\frac{\left[x_n(t) - x_{AT,1}\right]^2}{x_{AT,2} - x_{AT,1}} \tag{14}$$

Applying the instantaneous values of S_n, $Z_{T,n}$ and $Z_{S,n}$ to the system of equations formed by (10) and (11), the voltage U_n and current I_n can be derived. Finally, the power loss in the electrification system $S_{L,n}$ and power in the traction transformer S_{TT} are evaluated in (15) and (16), respectively.

$$S_{L,n}(t) = [Z_{TT} + Z_n(t)]|I_n(t)|^2 \tag{15}$$

$$S_{TT}(t) = S_n(t) + S_{L,n}(t) \tag{16}$$

In the current operation of high-speed lines, it is unlikely that two consecutive trains in the same direction will run within the same electrification section [55]. However, there are frequent crossings of two trains running in opposite directions. In these cases, both trains concur within the same electrification section for an interval of time.

Fig. 3 shows the equivalent circuit at an instant of the concurrence interval of two trains within an electrification section. The traction circuit of train 2 crosses the supply subsection of train 1. Since both trains run on different tracks, the current I_2 is divided into two equal parts within the supply subsection of train 1. If the supply subsections of the two trains are different, the transmission impedances $Z_{T,12(1)}$ and

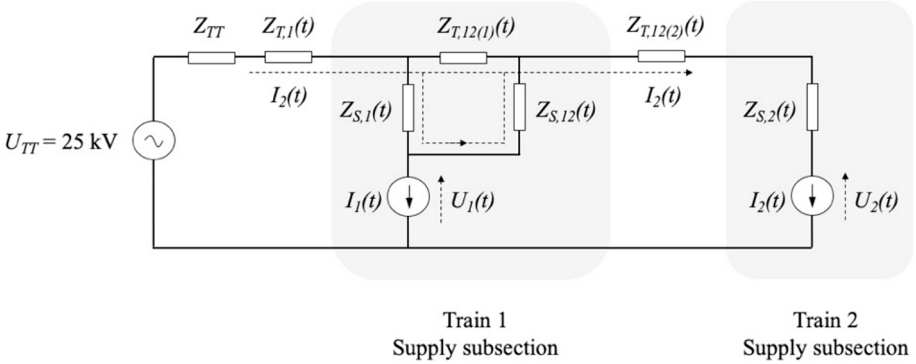

Fig. 3. Equivalent circuit for a section with two concurrent trains in the approximate 2x25 kV system model.

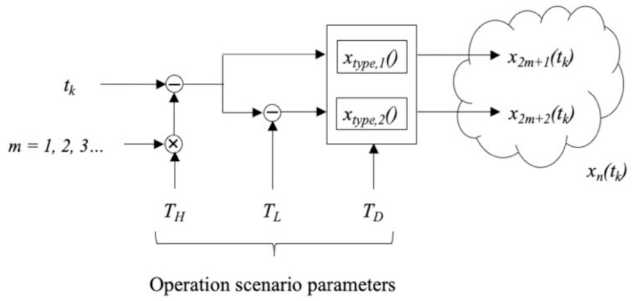

Fig. 4. First algorithm. The trajectories of all services are generated from the parameters defining the operating scenario.

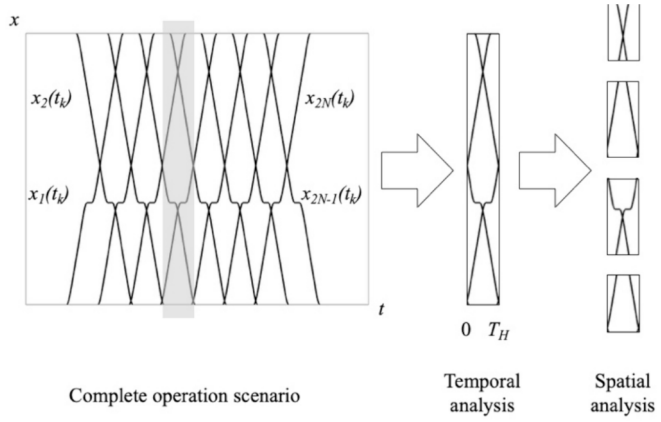

Fig. 5. Temporal and spatial analysis of the operation scenario.

$Z_{T,12(2)}$ are calculated in (17) and (18), respectively. On the contrary, the transmission impedances $Z_{T,12(1)}$ and $Z_{T,12(2)}$ are zero.

$$Z_{T,12(1)}(t) = \overline{Z}_{i\pm}\left[(x_{AT,2(1)} - x_{AT,1(1)})\right] \tag{17}$$

$$Z_{T,12(2)}(t) = \overline{Z}_{i\pm}\left[(x_{AT,1(2)} - x_{AT,2(1)})\right] \tag{18}$$

Exploiting the linearity of the traction circuit in (11), the superposition principle can be applied to evaluate the effect of the concurrency of the two trains within the electrification section. The mutual effects caused by the overlapping of their traction circuits are collected in the impedance matrix $\boldsymbol{Z}$ [56].

$$\begin{bmatrix} 25 \\ 25 \end{bmatrix} = \begin{bmatrix} U_1(t) \\ U_2(t) \end{bmatrix} + \left\{ \begin{bmatrix} Z_{TT} \\ Z_{TT} \end{bmatrix} + \boldsymbol{Z}(t) \right\} \begin{bmatrix} I_1(t) \\ I_2(t) \end{bmatrix} \tag{19}$$

The instantaneous values of the currents and voltages in the traction chains of the two concurrent trains are deduced in the system of equations formed by (10) and (19). Then, the instantaneous power loss in the electrification system S_L is calculated in (20) as the sum of the power loss in both traction circuits considered individually $S_{L,1}$ and $S_{L,2}$, plus the mutually induced power losses due to their overlapping S_X. The mutual power loss S_X can be calculated as shown in (21)-(23). Finally, the instantaneous power in the traction transformer S_{TT} within the concurrence interval can be evaluated in (24).

$$S_L(t) = S_{L,1}(t) + S_{L,2}(t) + S_X(t) \tag{20}$$

$$S_X(t) = S_{X,12}(t) + S_{X,21}(t) \tag{21}$$

$$S_{X,12}(t) = [Z_{TT} + Z_{12}(t)]I_1^*(t)I_2(t) \tag{22}$$

$$S_{X,21}(t) = [Z_{TT} + Z_{21}(t)]I_2^*(t)I_1(t) \tag{23}$$

$$S_{TT}(t) = S_1(t) + S_2(t) + S_L(t) \tag{24}$$

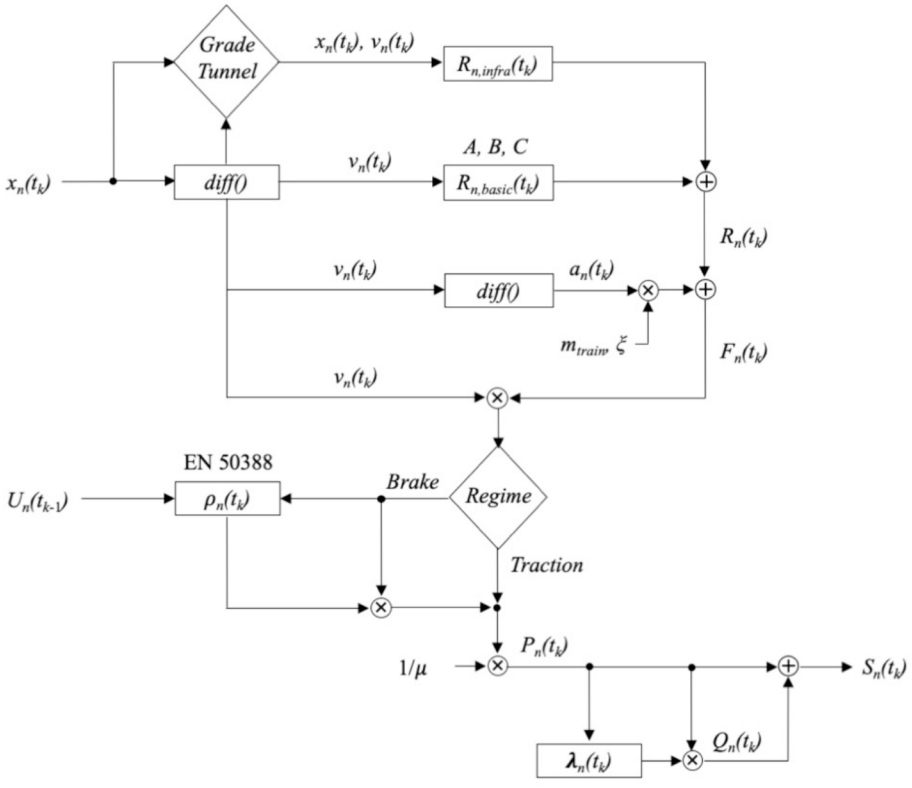

Fig. 6. Second algorithm. The electrical power of each train is deduced from its trajectory.

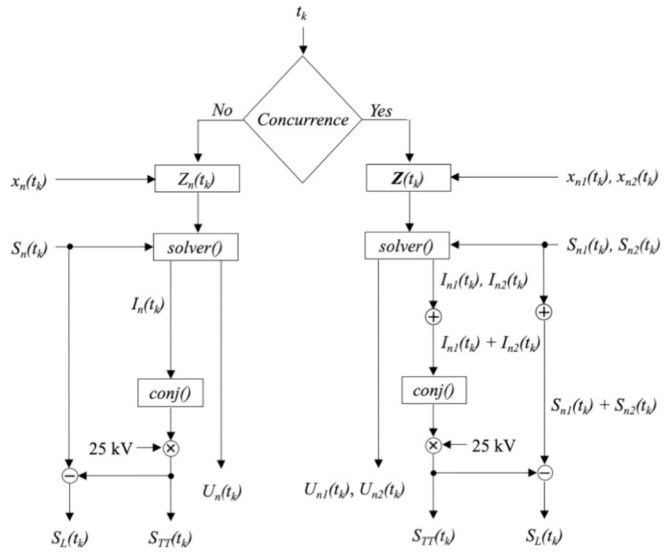

Fig. 7. Third algorithm. The electrical power transmission loss in the electrification system and the electrical power in the traction transformer are calculated.

3. Simulation algorithms

The dynamic simulation of the complete railway system during the operation of a transportation plan is performed by solving the presented mathematical models at each instant. As shown in Fig. 4, a first algorithm takes as input parameters the headway T_H, the layover time T_L and the dwell time T_D. Applying expressions (1) and (2), the trajectory of each service $x_n(t_k)$ in the defined operating scenario is obtained.

The periodic structure of the transportation plan makes the simulation redundant during the entire service period. Therefore, it is sufficient to run the dynamic simulation within a time window of T_H duration and extrapolate the results by cyclic repetition. Besides, the autonomous operation of each electrification section makes it possible to sectorize the dynamic simulation into independent parts. The temporal and spatial analyses (Fig. 5) reduce the computational burden and make the recurrent use of dynamic simulations feasible.

Fig. 6 shows the operations performed by the second algorithm developed for this dynamic simulation. In the upper part, expressions (3)-(5) are applied to solve the mechanical side of the mathematical model taking as input the trajectory $x_n(t_k)$ of each service. In the lower part, expressions (6)-(9) are evaluated, which represent the electromechanical conversion performed in the traction chain. Finally, this second algorithm calculates the electrical power $S_n(t_k)$ of each service.

Fig. 7 presents the calculations performed by the third algorithm to obtain the power loss in the electrification system $S_L(t_k)$ and the power of the traction transformer $S_{TT}(t_k)$. First, this algorithm checks at each instant whether there is concurrency within the electrification section. If only one train runs through the electrification section, expressions (10)-(16) of the mathematical model of the electrification system are applied. Conversely, if two trains run within the electrification section, expressions (17)-(24) are evaluated.

4. Case studies

In this section, three transportation plans are simulated to evaluate the effect of scheduling modifications on losses in the electrification system.

4.1. Case study 1. Short distance service

This case study simulates and analyzes the set of operating scenarios of a transportation plan generated by varying the layover T_L. The services run in both directions between two stations A and B, 100 km distant from each other. The track profile between the two stations is horizontal and there are no tunnels. As shown in Fig. 8, the electrification infrastructure follows the 2x25 kV system with two electrification sections of 50 km length each. Both sections are fed respectively by two traction transformers housed in a traction substation located at kilometer point 50. Along each electrification section there are three equispaced autotransformers.

The transportation services are provided by trains with a maximum power of 8 MW, a mass of 324 t, a length of 200 m, a maximum speed of 300 km/h, and traction and braking characteristics as given in [57]. The type trajectories proposed for this case study consist of three phases: acceleration at maximum traction force, cruise at constant speed, and deceleration at maximum braking force. The travel time in both directions has been set at 25 min and –given the traction and braking capabilities of the trains– the speed in the cruise phase should be 270 km/h. The transportation plan is provided continuously and the departure times of consecutive services in each direction follow a T_H headway of 30 min.

The symmetry of the trajectories and infrastructure results in a new symmetry in the scenarios generated in both sections. Then, the operation in section 1.1 for T_L is identical to the operation in section 1.2 for 30–T_L. The trajectories of services for $T_L = 15$ min have been plotted in Fig. 9. As can be seen, the operation scenarios in both sections are identical. Therefore, it is sufficient to simulate for section 1.1 and extrapolate the results for section 1.2.

The active power P_{TT} in the traction transformer of section 1.1 for $T_L = 15$ min is shown in the upper part of Fig. 10. The acceleration phase of the 2 m + 1 service takes place between minutes 0 and 4.2 and the braking phase of the 2 m service between minutes 7.2 and 10. Acceleration and braking at constant torque –at low speed– temporarily vary the power exchanged between the train and the traction transformer. On the other hand, the power in the traction transformer remains stable when

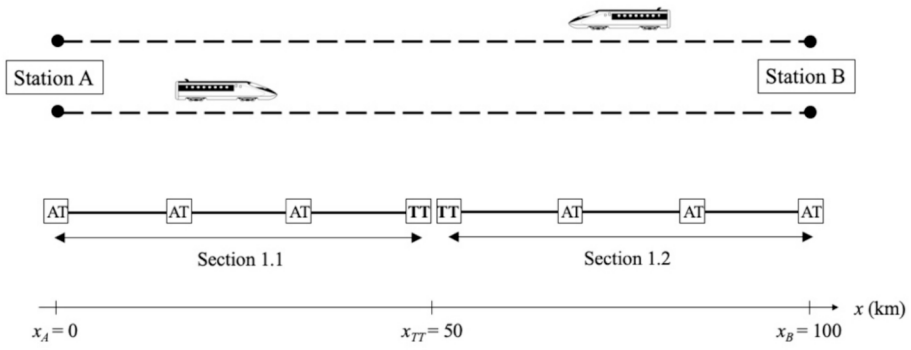

Fig. 8. Route and electrification system of the transportation plan simulated in the first case study.

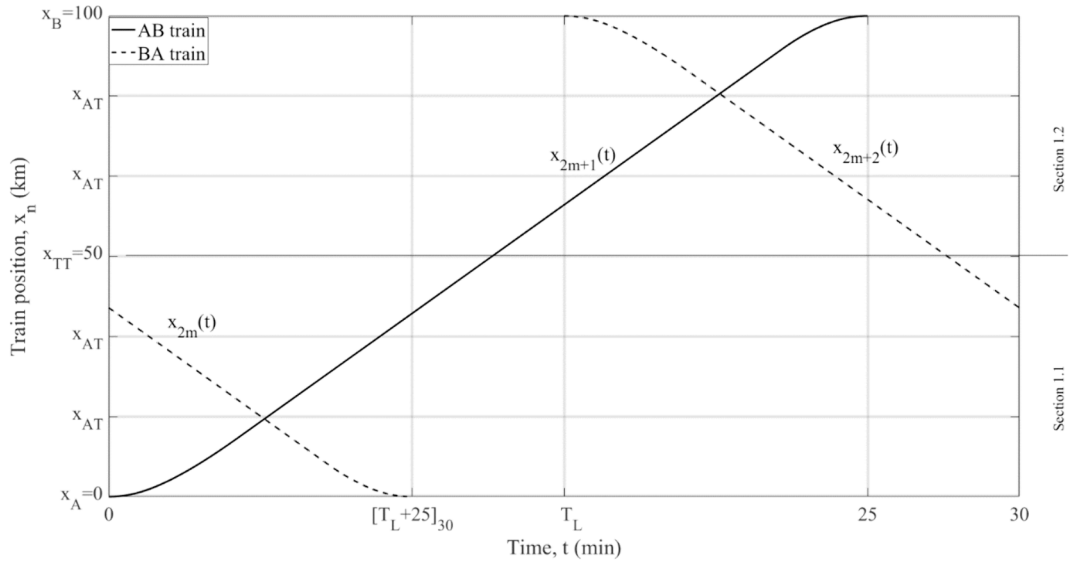

Fig. 9. Service trajectories contained within the simulation time window of the first case study for $T_L = 15$ min.

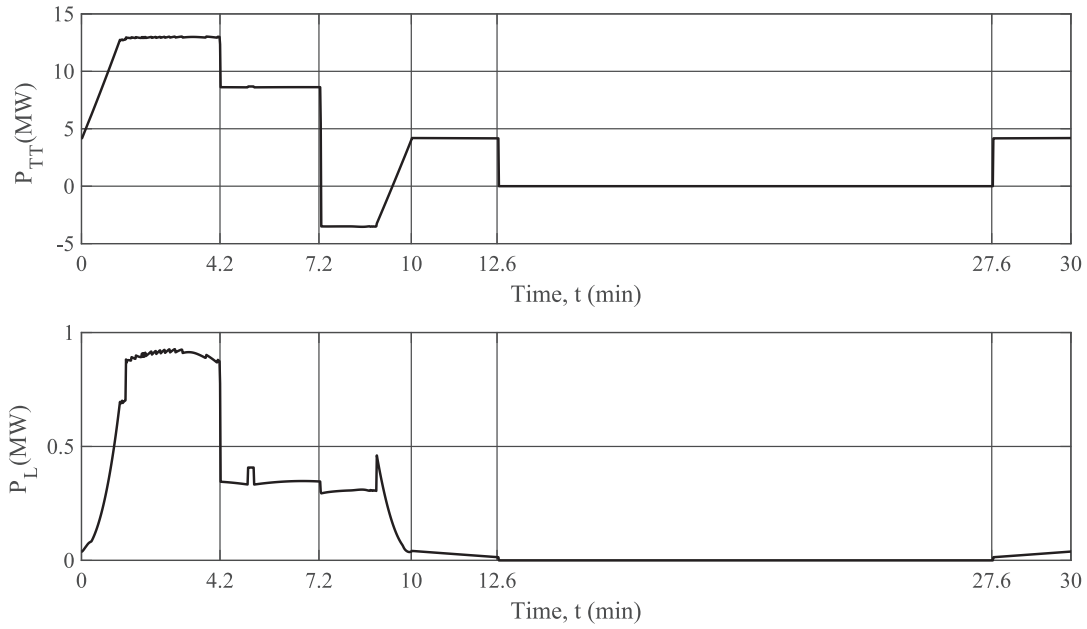

Fig. 10. Instantaneous active power in the first traction transformer and instantaneous active power loss in section 1.1 obtained from the simulation of the operation scenario corresponding to $T_L = 15$ min.

trains accelerate or brake at constant power –at high speed. Additionally, the power supplied by the traction transformers remains stable during the cruising phases as forward resistances are constant. Finally, both trains change sections at minutes 12.6 and 27.6.

As stated in (20), the power loss can be expressed as the sum of the power losses in the traction circuits of the trains individually considered plus the effect resulting from the overlapping of the traction circuits. The total active power loss in section 1.1 and layover time T_L of 15 min has been represented in the lower part of Fig. 10. It can be seen that the active power loss is clearly higher during acceleration and braking phases than during cruising phases, i.e., when circulating currents are more intense. Furthermore, according to (16), the distances between the trains and the traction transformer have an influence on the trend of active power losses in the traction circuits.

According to (21)-(23), the effect of overlapping when both trains are simultaneously accelerating –or braking– is to increase power losses in the traction circuits. Otherwise, the power losses are decreased when one train is braking, and the other one is accelerating. Thus, as can be checked in Fig. 10, the overlapping decreases the power loss in the traction circuits during the time interval 7.2–10 min as a direct power flow is established between the braking train –service 2 m– and the accelerating train –service 2 $m + 1$–.

Choosing a different value for the layover time T_L temporarily shifts the trajectory of the even services and modifies the overlapping loss during concurrency intervals within the simulation window. As mentioned above, a complete set of equivalent operating scenarios is obtained from the variation of T_L from 0 to 29 min. Fig. 11 plots the relative values of the total active power loss for each operating scenario. As can be seen, central symmetry emerges when adding the losses of both sections. The total transmission losses in simulated scenarios range between 3.73 % and 5.45 % of the energy supplied by the traction transformers. Consequently, the efficient scheduling strategy presented

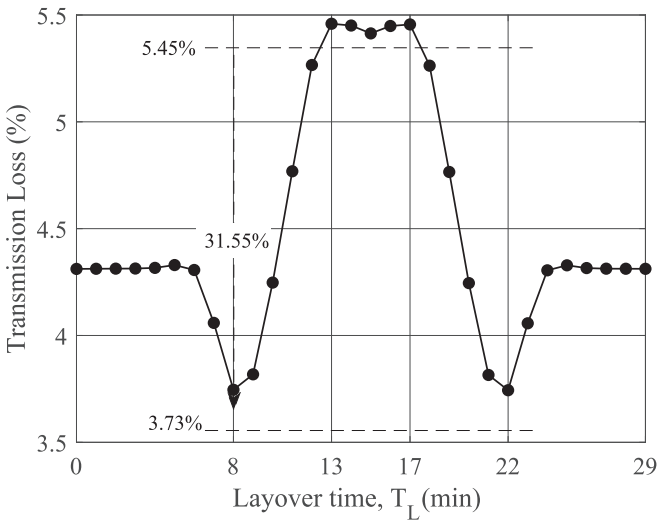

Fig. 11. Total transmission losses in the first case study for each of the 30 equivalent operating scenarios.

allows for loss savings of up to 31.55 % for this transportation plan.

4.2. Case study 2. Medium distance service

In this second case study, a transportation plan between two stations A and B, 200 km apart, is analyzed. The track follows the same design presented in the first case study. As shown in Fig. 12, the electrification infrastructure consists of four sections equipped with three equispaced autotransformers. Sections 2.1 and 2.2 are fed by two transformers located at the traction substation at kilometer point 50. Sections 2.3 and 2.4 are fed by two transformers located at the traction substation at kilometer point 150. The type trajectories between the two stations consist of three phases. The speed during the cruise phase is 270 km/h and the travel time is 47 min. As in the first case study, the T_H headway between two consecutive services in the same direction is 30 min.

Considering the symmetry of the trajectories of the trains and the infrastructure, it is sufficient to simulate the operation in sections 2.1 and 2.2, and extrapolate the results to sections 2.3 and 2.4, respectively. Additionally, the acceleration and braking phases and the topology of the electrification system are the same as those described in the first case study. Consequently, the values of transmission losses in the extreme sections 2.1 and 2.4 are equal to those obtained for sections 1.1 and 1.2, respectively. However, the operation scenarios are laterally shifted since in this second case study the travel time is 22 min longer.

The active power P_{TT} in the traction transformer of section 2.2 for T_L = 23 min is shown in the upper part of Fig. 13. This section is traversed by trains –applying constant traction– in cruising phase between minutes 12.6 and 27.9. The active power loss P_L in section 2.2 has been represented in the lower part of Fig. 13. The observed trends in active power losses are consistent with the trajectory of the trains. According to (22)-(24), the coincidence of two trains in section 2.2 between minutes 16.8 y 23.8 produces power loss due to overlapping.

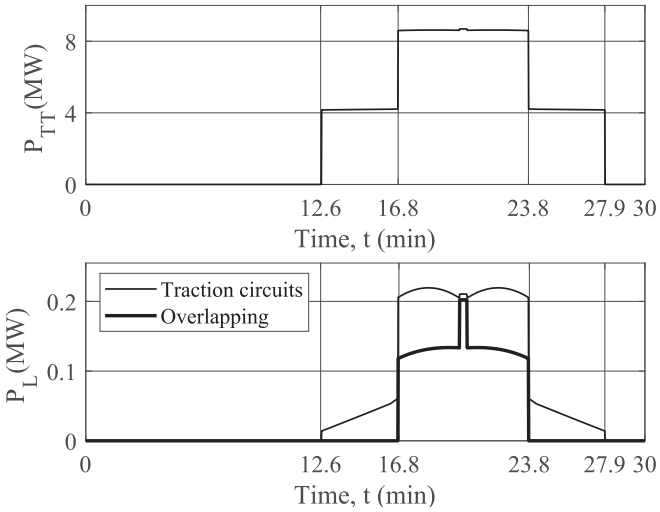

Fig. 13. Instantaneous active power in the first traction transformer and instantaneous active power loss in section 2.2 obtained from the simulation of the operation scenario corresponding to T_L = 23 min.

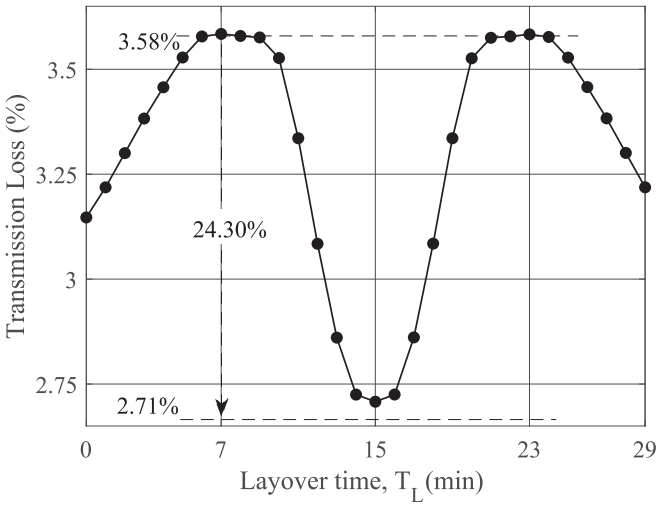

Fig. 14. Total transmission losses in the second case study for each of the 30 equivalent operating scenarios.

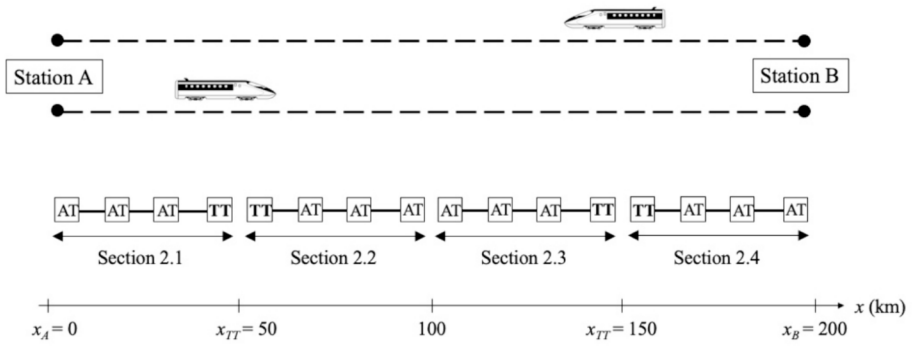

Fig. 12. Route and electrification system of the transportation plan simulated in the second case study.

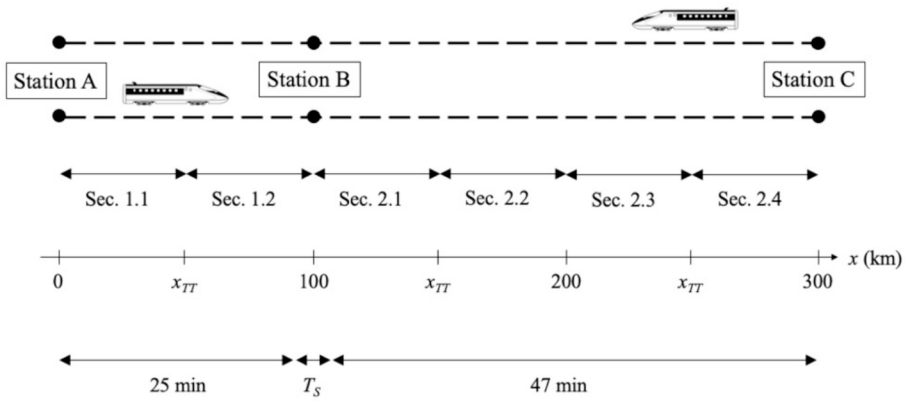

Fig. 15. Route, electrification system and travel times of the transportation plan simulated in the third case study.

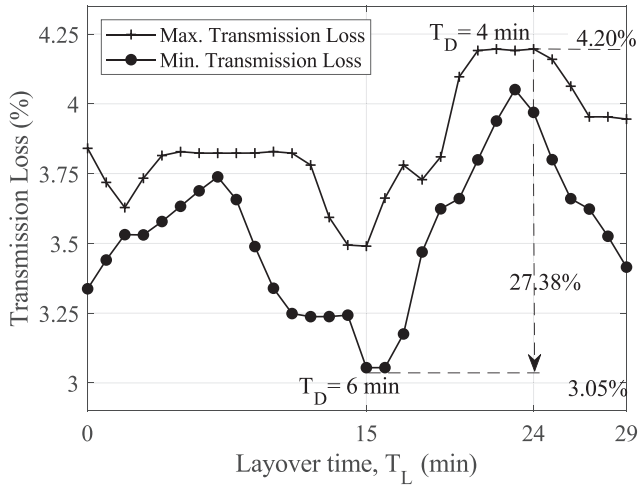

Fig. 16. Maximum and minimum total transmission losses in the third study case for the 210 equivalent operating scenarios.

As can be seen in Fig. 14, total transmission losses in the set of equivalent operating scenarios analyzed range between 2.71 % and 3.58 % of the energy supplied by the traction transformers. Consequently, the efficient scheduling strategy presented allows savings of up to 24.30 % in the transmission losses of this transportation plan.

4.3. Case study 3. Long distance service

In this third case study, a long-distance transportation plan is considered. The operation is developed on the infrastructure resulting from the union of the two previous case studies. The rail services are extended between stations A, B and C, as shown in Fig. 15. The type trajectories presented in the first and the second case study are used on the routes between A and B, and B and C, respectively. The dwell time at intermediate station B is T_D. The headway T_H between two consecutive services in the same direction is 30 min.

The transportation plan of this third case study can be decomposed into two pieces and the efficient scheduling strategy can be deduced from the results of the previous case studies. The equivalent layover times between the even services and odd services in each of the two pieces are deduced from the travel times, layover time T_L and dwell time T_D. Then, the layover time between stations A and B is $T_{L1} = [T_L + T_D + 47]_{30}$, and the layover time between stations B and C is $T_{L2} = [T_L + T_D - 25]_{30}$. Applying T_{L1} and T_{L2} to the results shown in Fig. 11 and Fig. 14, respectively, the transmission losses corresponding to each pair (T_L, T_D) can be obtained.

In this third case study, the search space for operating scenarios is more extensive. For each layover time T_L, there are as many operating scenarios as possible dwell time T_D values. Fig. 16 shows the minimum and maximum transmission loss scenarios found in $T_D \in$ [2,8] min for each T_L.

As can be noticed, the efficient scheduling strategy presented can achieve savings of up to 27.38 % in transmission losses for this transportation plan. These savings lie between the values obtained in the two previous case studies.

5. Conclusions

In this paper, power transmission losses of high-speed transportation plans are evaluated through dynamic simulations of the 2x25 kV electrification system. Spatial and temporal distribution of running trains are translated into mechanical terms and power exchanges within the railway system are evaluated. For each transportation plan, a set of equivalent operating scenarios has been generated by means of slight variations of the scheduling for each plan. Although the energy consumption of the trains is the same in all scenarios of each set, overall transmission losses differ significantly depending on the mode of train concurrency within electrification sections. It can be concluded that there is a simple efficient scheduling strategy that allows to operate a transportation plan in the minimum transmission loss scenario that can be implemented immediately and without relevant costs for the operator. This strategy preserves the service offered to passengers and the fleet size required for the operation. The energy savings obtained are continuous over time as the rail operation consistently replicates the scheduled timetables. Future research is aimed at implementing more complete models, and to consider the Integration of Energy Storage and Renewable Energy Sources.

CRediT authorship contribution statement

Jesus Riego-Martinez: Writing – original draft, Software, Methodology, Data curation, Conceptualization. **Marcelo Perez-Alonso:** Validation, Supervision, Conceptualization. **Oscar Duque-Perez:** Writing – review & editing, Validation, Supervision, Conceptualization.

Declaration of competing interest

The authors declare that they have no known competing financial interests or personal relationships that could have appeared to influence the work reported in this paper.

Data availability

The data that has been used is confidential.

References

[1] International Energy Agency and the International Union of Railways, "Railway Handbook on Energy Consumption and CO2 Emissions", 2017, pp. 17-27.
[2] Pu H, Cai L, Song T, et al. Minimizing costs and carbon emissions in railway alignment optimization: a bi-objective model. Transp Res Part D: Transp Environ 2023;116:103615.
[3] International Union of Railways, "High Speed Rail. Fast Track to Sustainable Mobility", 2018, pp. 41-57.
[4] Feng X, Zhang H, Ding Y, et al. A review study on traction energy saving of rail transport. Discret Dyn Nat Soc 2013.
[5] Brenna, M., Bucci, V., Falvo, M.C., et al., "A review on energy efficiency in three transportation sectors: Railways, electrical vehicles and marine", Energies, 2020, 13 (9), art. no. 2378. DOI: 10.3390/en13092378.
[6] Scheepmaker GM, Goverde RM, Kroon LG. Review of energy-efficient train control and timetabling. Eur J Oper Res 2017;257(2):355–76.
[7] Cao Y, et al. Trajectory optimization for high-speed trains via a mixed integer linear programming approach. IEEE Trans Intell Transp Syst 2022;23(10): 17666–76.
[8] Montrone T, Pellegrini P, Nobili P. Real-time energy consumption minimization in railway networks. Transp Res Part D: Transp Environ 2018;65:524–39.
[9] Xie J, Zhang J, Sun K, et al. Passenger and energy-saving oriented train timetable and stop plan synchronization optimization model. Transp Res Part D: Transp Environ 2021;98:102975.
[10] Botte M, D'Acierno L, Di Pasquale A, Mottola F, Pagano M. In: October). Performance Improvements of Traction Power Systems by Coordinating the Motion of a Fleet of Metro Trains in terms of Layover Time. IEEE; 2021. p. 1–6.
[11] Khodaparastan M, Mohamed AA, Brandauer W. Recuperation of regenerative braking energy in electric rail transit systems. IEEE Trans Intell Transp Syst 2019; 20(8):2831–47.
[12] Wang X, Tang T, Su S, et al. An integrated energy-efficient train operation approach based on the space-time-speed network methodology. Transp Res Part E: Logistics Transp Rev 2021;150.
[13] Ahmadi S, Dastfan A, Assili M. Improving energy-efficient train operation in urban railways: employing the variation of regenerative energy recovery rate. IET Intel Transport Syst 2017;11(6):349–57.
[14] Sun P, et al. Timetable optimization for maximization of regenerative braking energy utilization in traction network of urban rail transit. Comput Ind Eng 2023; 183:109448.
[15] Zhang L, et al. Real-time energy saving optimization method for urban rail transit train timetable under delay condition. Energy 2022;258:124853.
[16] Wu C, et al. A two-step method for energy-efficient train operation, timetabling, and onboard energy storage device management. IEEE Trans Transp Electrif 2021; 7(3):1822–33.
[17] Pena-Alcaraz M, Fernandez A, Cucala AP, Ramos A, Pecharroman RR. Optimal underground timetable design based on power flow for maximizing the use of regenerative-braking energy. Proc Inst Mech Eng Part F J Rail Rapid Transit 2011; 12(2):374–83.
[18] Yang S, Liao F, Wu J, et al. A bi-objective timetable optimization model incorporating energy allocation and passenger assignment in an energy-regenerative metro system. Transp Res B Methodol 2020;133:85–113.
[19] Liu H, Zhou M, Guo X, et al. Timetable optimization for regenerative energy utilization in subway systems. IEEE Trans Intell Transp Syst 2019;20(9):3247–57.
[20] Zhou W, Huang Y, Deng L, Qin J. "Collaborative optimization of energy-efficient train schedule and train circulation plan for urban rail". Energy 2023;263(Part A): 125599.
[21] Kuppusamy P, et al. Deep learning based energy efficient optimal timetable rescheduling model for intelligent metro transportation systems. Phys Commun 2020;42:101131.
[22] Huang K, Liao F, Gao Z. An integrated model of energy-efficient timetabling of the urban rail transit system with multiple interconnected lines. Transportation Research Part C: Emerging Technologies 2021;129:103171.
[23] Yang S, et al. An efficient train timetable scheduling approach with regenerative-energy supplementation strategy responding to potential power interruptions. IEEE Trans Intell Transp Syst 2021;23(9):14267–82.
[24] Du G, et al. Multi-objective optimization of traction substation converter characteristic and train timetable in subway systems. IEEE Trans Transp Electrif 2022. timet.
[25] Su S, Wang X, Cao Y, Yin J. An energy-efficient train operation approach by integrating the metro timetabling and eco-driving. IEEE Trans Intell Transp Syst 2019;21(10):4252–68.
[26] Liao J, Yang G, Zhang S, Zhang F, Gong C. A Deep Reinforcement Learning Approach for the Energy-Aimed Train Timetable Rescheduling Problem Under Disturbances. IEEE Trans Transp Electrif Dec. 2021;7(4):3096–109. https://doi.org/10.1109/TTE.2021.3075462.
[27] Yin J, Yang L, Tang T, Gao Z, Ran B. Dynamic passenger demand oriented metro train scheduling with energy-efficiency and waiting time minimization: Mixed-integer linear programming approaches. Transp Res B Methodol 2017;97:182–213.
[28] D'Acierno L. Botte, M, "Railway System Design by Adopting the Merry-Go-Round (MGR) Paradigm". Sustainability 2021;13:2033. https://doi.org/10.3390/su13042033.
[29] Botte M, D'Acierno L, Di Pasquale A, Mottola F, Pagano M. Optimal Allocation of Layover Time in a Smart DC Railway Metro Traction System. IEEE Trans Veh Technol 2024.
[30] Xiao Z, Wang Q, Sun P, You B, Feng X. Modeling and Energy-Optimal Control for High-Speed Trains. IEEE Trans Transp Electrif June 2020;6(2):797–807.
[31] Restel F, Wolniewicz L, Mikulčić M. Method for designing robust and energy efficient railway schedules. Energies 2021;14(24):8248.
[32] Kierzkowski A, Haładyn S. Method for Reconfiguring Train Schedules Taking into Account the Global Reduction of Railway Energy Consumption. Energies 2022;15 (5):1946.
[33] Wang P, et al. Improving the utilization of regenerative energy and shaving power peaks by railway timetable adjustment. IEEE Trans Intell Transp Syst 2022;23(9): 15742–54.
[34] Urbaniak M, Kardas-Cinal E. Optimization of Train Energy Cooperation Using Scheduled Service Time Reserve. Energies 2021;15(1):119.
[35] Restel F, Haładyn SM. The Railway Timetable Evaluation Method in Terms of Operational Robustness against Overloads of the Power Supply System. Energies 2022;15(17):6458.
[36] Sun Y, Cao C, Wu C. Multi-objective optimization of train routing problem combined with train scheduling on a high-speed railway network. Transportation Research Part C: Emerging Technologies 2014;44:1–20.
[37] Pan Z, et al. Integrated timetable optimization for minimum total energy consumption of an AC railway system. IEEE Trans Veh Technol 2020;69(4): 3641–53.
[38] Riego-Martinez J, Perez-Alonso M, Duque-Perez O. Influence of the rail electrification system topology on the energy consumption of train trajectories. IET Renew Power Gener 2020;14(18):3589–98.
[39] Timetable recovery margins to guarantee timekeeping - Recovery margins, UIC Leaflet 451-1, 2000.
[40] Liebchen C. Symmetry for Periodic Railway Timetables. Electron Notes Theor Comput Sci 2004;92:34–51.
[41] Pröhl, L., "OPEUS Deliverable DO2. 1-OPEUS simulation methodology", EU-project Modelling and strategies for the assessment and OPtimisation of Energy USage aspects of rail innovation, 2017.
[42] Chen X, Li K, Zhang L, Tian Z. Robust Optimization of Energy-Saving Train Trajectories Under Passenger Load Uncertainty Based on p-NSGA-II. IEEE Trans Transp Electrif March 2023;9(1):1826–44. https://doi.org/10.1109/TTE.2022.3194698.
[43] Pritchard JA, Preston J. Understanding the contribution of tunnels to the overall energy consumption of and carbon emissions from a railway. Transp Res Part D: Transp Environ 2018;65:551–63. https://doi.org/10.1016/j.trd.2018.09.010.
[44] Wang K, Hu H, Chen C, et al. A simulation platform to assess comprehensive power quality issues in electrified railways. International Journal of Rail Transportation 2018;6(4):233–54.
[45] Wu Q, Cole C, Spiryagin M, et al. Freight train air brake models. International Journal of Rail Transportation 2023;11(1):1–49. https://doi.org/10.1080/23248378.2021.2006808.
[46] Railway Applications - Power supply and rolling stock - Technical criteria for the coordination between power supply (substation) and rolling stock to achieve interoperability, CENELEC EN 50388, 2012.
[47] H. Douglas F. Schmid C. Roberts et al. Evaluation of Permanent Magnet Motor energy saving technology for different types of railways 2016 Birmingham 123 129.
[48] He Z, Zheng Z, Hu H. Power quality in high-speed railway systems. International Journal of Rail Transportation 2016;4(2):71–97.
[49] Minucci, S., Pagano, M., Proto, D., "Model of the 2×25kV high speed railway supply system taking into account the soil-air interface", International Journal of Electrical Power & Energy Systems, 2018, 95, 2018, pp. 644-652, ISSN 0142-0615, doi.org/10.1016/j.ijepes.2017.09.017.
[50] Mariscotti A, Pozzobon P, Vanti M. Simplified Modeling of 2x25-kV AT Railway System for the Solution of Low Frequency and Large-Scale Problems. IEEE Trans Power Delivery 2006;22(1):296–301.
[51] Serrano-Jiménez D, Abrahamsson L, Castaño-Solís S, et al. Electrical railway power supply systems: Current situation and future trends. Int J Electr Power Energy Syst 2017;92:181–92.
[52] Brenna M, Foiadelli F, Zaninelli D. Electromagnetic model of high-speed railway lines for power quality studies. IEEE Trans Power Syst 2010;25(3):1301–8.
[53] Mohamed B, Arboleya P, El-Sayed I, et al. High-speed 2×25 kV traction system model and solver for extensive network simulations. IEEE Trans Power Syst 2019; 34(5):3837–47.
[54] Brenna M, Foiadelli F, Zaninelli D. "AC Systems at Mains Frequency" in Electrical railway transportation systems. Hoboken, NJ, USA: Wiley-IEEE Press; 2018. p. 209–23.
[55] Kiessling F, Puschmann R, Schmieder A, et al. "Interaction of pantograph and overhead contact line" in Contact Lines for Electric Railways: Planning. 3rd ed. Implementation, Maintenance, Publicis MCD Verlag, Germany: Design; 2018.
[56] Pilo E, Rouco L, Fernandez A, et al. A monovoltage equivalent model of bi-voltage autotransformer-based electrical systems in railways. IEEE Trans Power Delivery 2012;27(2):699–708.
[57] Fernández-Rodríguez A, Fernández-Cardador A, Cucala PA. Real time eco-driving of high-speed trains by simulation-70 dynamic multi-objective optimization. Simul Model Pract Theory 2018;84:50–68.